Green Chemistry Letters and Reviews

ISSN: (Print) (Online) Journal homepage: www.tandfonline.com/journals/tgcl20

Green synthesis of copper-based nanoparticles using coffee husk and investigation of its antifungal activity and phytotoxicity *in vitro*

Dao Thi Le, Tho Phuoc Tran, Tuan Nghiem Anh Le, Quang Ngoc Tran, Hien Quoc Nguyen & Du Duy Bui

To cite this article: Dao Thi Le, Tho Phuoc Tran, Tuan Nghiem Anh Le, Quang Ngoc Tran, Hien Quoc Nguyen & Du Duy Bui (2024) Green synthesis of copper-based nanoparticles using coffee husk and investigation of its antifungal activity and phytotoxicity *in vitro*, Green Chemistry Letters and Reviews, 17:1, 2432491, DOI: 10.1080/17518253.2024.2432491

To link to this article: https://doi.org/10.1080/17518253.2024.2432491

Published online: 28 Nov 2024.

GREEN CHEMISTRY LETTERS AND REVIEWS
2024, VOL. 17, NO. 1, 2432491
https://doi.org/10.1080/17518253.2024.2432491

Green synthesis of copper-based nanoparticles using coffee husk and investigation of its antifungal activity and phytotoxicity *in vitro*

Dao Thi Le[a], Tho Phuoc Tran[b], Tuan Nghiem Anh Le[b], Quang Ngoc Tran[c,d], Hien Quoc Nguyen[e] and Du Duy Bui[a,b]

[a]Graduate University of Science and Technology, Vietnam Academy of Science and Technology, Hanoi, Vietnam; [b]Institute of Applied Materials Science, Vietnam Academy of Science and Technology, Ho Chi Minh City, Vietnam; [c]Center for Innovative Materials & Architectures, Ho Chi Minh City, Vietnam; [d]Vietnam National University, Ho Chi Minh City, Vietnam; [e]Vietnam Atomic Energy Institute, Hanoi, Vietnam

ABSTRACT

Coffee husks (CH) are waste with abundant reserves in Vietnam. This type of waste is mainly composed of cellulose, hemicellulose, minerals, and some reducing active ingredients such as polyphenols, reducing sugars, and lignin, so it is suitable for use as raw material for producing organic fertilizer for reuse in agriculture. In this study, we present a new method to quickly treat CH by directly using it as a reducing and stabilizing agent to green synthesize the $Cu/Cu_2O/CH$ nanocomposite with Cu content of 3% (w/w). The size of the obtained Cu/Cu_2O nanoparticles (NPs) determined from scanning electron microscope (SEM) images was 54.6 ± 28.2 nm. The characteristic properties of the materials are determined by X-ray diffraction (XRD), Fourier transform infrared spectroscopy (FTIR), energy dispersive X-ray (EDX), and elemental mapping. In the *in vitro* experiment, the $Cu/Cu_2O/CH$ nanocomposite achieved 93.52% effectiveness against *Phytophthora capsici* at a concentration of 55 mg/L Cu, and the inhibitory concentration 50% (IC_{50}) value was determined to be 19.67 mg/kg. Furthermore, the obtained the $Cu/Cu_2O/CH$ nanocomposite with a content of ~3% Cu (w/w) can degrade caffeine, a toxic substance to plants in CH by ~95%. The $Cu/Cu_2O/CH$ nanocomposite can be potentially used as a disease control agent and micronutrient fertilizer for plants.

ARTICLE HISTORY
Received 5 September 2024
Accepted 15 November 2024

KEYWORDS
Copper-based nanocomposite; coffee husk; green synthesis; *Phytophthora capsici*; mung bean

1. Introduction

Coffee husk (CH) is a waste from coffee beans which has abundant reserves of about 1.78 million tons in Vietnam (2022–2023) (1). The layer surrounding the coffee beans after being removed is called CH, it is often used as fuel for drying activities (2). Coffee husks make up ~14% of the bean's weight (3), so in Vietnam, about 0.25 million tons of CH are discharged into the environment, which needs proper treatment. According to research by Gouvea et al. (4), the composition of CH depends on the variety and cultivation conditions, CH contains 58–85% total carbohydrates, 43% cellulose, 7% hemicellulose, 8–11% protein, 0.5–3.0% lipids, 3–7% minerals, 9% lignin, ~5% tannins, and ~1% caffeine.

On the other hand, CH contains several biologically active substances with antioxidant properties such as reducing sugars and polyphenol compounds. The composition of bioactive substances in plants depends

CONTACT Du Duy Bui vina9802@gmail.com Institute of Applied Materials Science, Vietnam Academy of Science and Technology, Ho Chi Minh City 700000, Vietnam

greatly on the variety, genotype, cultivation method, soil, and post-harvest processing method (5, 6). The reducing sugar content in CH is approximately 12% (7). Phenolic compounds contained in CH are 10.5% (8). The total content of phenolic compounds in CH calculated by gallic acid equivalent (GAE) is 184.79–382.97 mg GAE/100 g depending on the solvent and extraction method (9). Similarly, the total polyphenol content in Robusta CH is 16.54–97.89 mg CAE (chlorogenic acid equivalent)/g, mainly tannins 12.73–79.71 mg CE (catechin equivalent)/g (10). Total phenolic compounds in Robusta CH from Dak Lak province, Vietnam was 159 ± 9 mg GAE/g dry weight (11), and in Amazonian Robusta CH, it was 70.22 mg GAE/g (12). There are many processing methods to obtain coffee beans after harvest such as dry processing (drying and hulling), wet processing (soaking coffee cherries in water then hulling), and fermentation of coffee cherries and hulling. Processing methods affect the content of bioactive substances as well as the taste of coffee. Processing methods affect the quality and flavor of coffee (13), thus affecting the content of bioactive substances in the husk. In addition, the extraction method also affected the results of polyphenol content (10). Since CH contains polyphenol compounds, reducing sugars, and lignin, they are a potential reducing agent to reduce Cu^{2+} ions to Cu or Cu_2O in the nanocomposite preparation.

For a long time, Cu-based fungicides have been an important role in controlling pathogenic microorganisms on many crops such as fruit trees, vegetables, and cereals (14). Copper is also a micronutrient involved in many physiological processes of plants such as photosynthesis, enzyme activity, oxidative stress reactions, etc. (15), and increases the disease resistance of plants (16). However, the use of Cu compounds in bulk form at high concentrations in agriculture causes Cu accumulation in soil and water pollution (17). In the form of nanomaterial, Cu compounds have high antibacterial activity, abundant raw materials, and low production costs, and at the same time, Cu nanocomposite also provides micronutrients to increase agricultural productivity (18). In addition, copper nanoparticles (Cu NPs) are small in size and have highly antimicrobial activity (19). Thus, the use of Cu-based nanocomposite in agriculture can reduce the dosage by up to 80% compared to bulk materials (20) and have some other advantages such as low dosage, high efficiency, and low ecotoxicity (14).

In recent years, some authors have studied the effectiveness of Cu-based nanomaterials in resisting harmful plant microorganisms such as controlling 60.78–73.53% of late blight disease on tomatoes caused by *Phytophthora infestans* after 10 days (21), completely inhibiting *Xanthomonas axonopodis* causing leaf blight on pomegranate at a concentration of 0.2 ppm after 48 h, which is 10,000 times smaller than using CuOCl in the bulk form (22). To date, there have been many reports of Cu-based nanomaterials resisting many types of plant pathogens such as *Fusarium graminearum*, *Fusarium culmorum*, *Fusarium oxysporum*, *Fusarium equiseti*, *Alternaria alternata*, *Curvularia lunata*, and *Phoma destructive* (23, 24, 25). The antimicrobial mechanism of Cu-based NPs is due to the affinity of Cu for the carboxyl group on the surface of microorganisms (26, 27), Cu also stimulates the production of ROS, which damages and inactivates cell membranes, inactivates enzymes, and disrupts protein function of microorganisms (28, 29).

There are two approaches to the synthesis of Cu-based nanoparticles, particularly, the top-down and the bottom-up approaches. Each approach has its advantages and disadvantages, but the bottom-up approach is more popular because it facilitates control over the shape and size of the resulting nanoparticles (30, 31). The bottom-up approach focuses on four types of chemical reactions, namely reduction, hydrolysis, condensation, and oxidation. For Cu oxide NPs, it is necessary to hydrolyze the precursor followed by dehydration, whereas, in the case of Cu_2O nanoparticles preparation, it is necessary to reduce the Cu^{2+} precursor to Cu^{+} with a reducing agent, followed by hydrolysis (32).

The synthesis of Cu, Cu_2O, and CuO nanoparticles using chemical reductants is commonly used due to its high yield, however, the obtained materials contain harmful reductant residues (33). Currently, green chemistry methods using plant extracts as reductants and/or stabilizers in the preparation of Cu and Cu_2O nanoparticles have been developed. Mohamed et al. (34) synthesized Cu/Cu_2O nanoparticles with a size of 78 nm using polyphenol compounds (phenolics and flavonoids) from seedless dates as reductants. Ramesh et al. (2012) (35) used reducing sugars from *Manihot esculenta* leaf extract to synthesize Cu_2O nanoparticles with a size of 50–80 nm. Li et al. (2016) synthesized Cu_2O nanoparticles using lignin as a reductant and stabilizer (36). Similarly, Leng et al. (2016) used lignin to reduce $CuSO_4$ to Cu nanoparticles attached to graphene at 300°C (37). The method using natural reductants extracted from *Seripheidium quettense* or *Ipomoea aquatica* leaf extract to synthesize Ag nanoparticles was also studied by Nasar et al. (2019) (38) and Khan et al. (2020) (39). In addition, *Jatropha curcas* leaf extract was also used by Khan et al. (2022) to synthesize CuO nanoparticles with the ability against *Meloidogyne incognita* (40).

Stabilizers such as surfactants or polymers must be used to stabilize Cu nanoparticles. Currently, many types of solid stabilizers have been studied and used

to synthesize Cu and Cu_2O nanoparticles such as graphene (37), silica (41), wood (42), zeolite (43), and cellulose (44). CH contains polyphenol compounds, reducing sugars, large amounts of cellulose and hemicellulose biomass, so it is suitable for use as a reducing agent and stabilizer to synthesize Cu and Cu_2O nanocomposite, which have the potential to be used as a fertilizer and antimicrobial agent for plants in the soil environment. On the other hand, the Cu and CuO nanoparticles can decompose caffeine pollutants (45, 46), a substance in CH that affects the growth and development of plants. Some photocatalytic nanoparticles have also been shown to be effective in decomposing caffeine in water such as ZnO (47), Fe_2O_3 (48), and TiO_2 (49). Cu_2O has a narrow band gap, strong visible light response, suitable conduction band position, and low cost, so it has the potential to be used as a photocatalyst to decompose pollutants in the environment (50). Caffeine in CH, if not removed, will reduce root growth by inhibiting protein production (51). Ferguson et al. (2015) confirmed that at concentrations of 100–1000 µmol, caffeine inhibited the growth of Wisconsin Fast Plant (52). Hanafi et al. (2020) reported that caffeine inhibited the growth of Ipomoea aquatic at concentrations of 0.05–0.35% (w/v) (53). Moreover, caffeine also inhibited germination and root elongation in crops such as soybean, peanut, alfalfa, white clover, wheat, corn, rye, lettuce, tomato, etc. (54).

In this study, we prepared Cu and Cu_2O nanoparticles using CH as a reducing and stabilizing agent. The obtained nanoparticles catalyze the decomposition of toxic caffeine in CH, aiming to be used as fertilizer, and plant-disease control agent in the soil environment.

2. Materials and methods

2.1. Materials

Chemicals used in the experiment were of analytical grade, including $CuSO_4$, NaOH, H_2SO_4, methanol, ethanol, hexane, $NaClO_2$, acetic acid (Xilong, China); 3,5-Dinitrosalicylic acid (DNSA) reagent, caffeine, dichloromethan, D-glucose, and Folin–Ciocalteu reagent (Merck, Germany); Robusta CH (Vietnam); *P. capsici* (Institute of Agriculture Science for Southern Viet Nam, Vietnam); Mung bean seeds (Rang Dong Seeds One Member Limited Liability Company, Vietnam). The deionized water was used throughout the experiment.

2.2. Methods

Extraction of the coffee husk (55): 10 g of CH was mixed with 100 mL of 80% methanol, the mixture was ground for 3 mins in a homogenizer and then transferred to a conical flask. The mixture was soaked for 24 h at room temperature, and then filtered through filter paper, the filtered extract was used to determine the total polyphenol and reducing sugar content.

Determination of total polyphenol (TP) content (9)**:** The CH extraction after reacting with the Folin–Ciocalteu reagent will be measured for optical density on a UV-Vis V630 spectroscopy (Jasco, Japan) at a wavelength of 765 nm. The experiment was repeated three times, using gallic acid as a standard for the calibration curve, the TP content (mg GAE/g CH) was presented as mean ± standard error (SE).

Determination of reducing sugar (RS) content (56)**:** DNSA reagent was prepared by dissolving 1 g of DNSA and 30 g of sodium-potassium tartaric acid in 80 mL of 0.5 N NaOH at 45°C, then cooled down to room temperature and diluted to 100 mL with deionized water. 2 mL of DNSA reagent was injected into a test tube containing 1 mL of CH extract and kept at 95°C for 5 min. The mixture was cooled, 7 mL of deionized water was added and the absorbance was measured on a UV-Vis V630 spectroscopy (Jasco, Japan) at a wavelength of 540 nm. The experiment was repeated three times, the RS content (mg GE/g) was presented as mean ± SE, using D-glucose as the standard for the standard curve.

Determination of total lignin content: 1 g CH was soaked in 15 mL of 72% H_2SO_4 for 2 h at room temperature to hydrolyze and dissolve carbohydrates. The mixture was diluted with 560 mL of deionized water to reduce the H_2SO_4 concentration to 3% and continued boiling for 4 h. The mixture was filtered, and washed with hot water until neutral pH was reached, then dried at 105°C to constant weight. After cooling in a desiccator, it was weighed to determine the insoluble lignin content according to formula (1) (57):

$$\text{Insoluble lignin } (\%) = 100 \times \frac{m}{m_0}, \qquad (1)$$

where m and m_0 (g) are the mass of insoluble lignin and CH, respectively.

The solution after filtration was used to determine the soluble lignin content by measuring the optical density on a UV-Vis V630 spectroscopy (Jasco, Japan) at a wavelength of 280 nm. The soluble lignin content was calculated according to formula (2) (58):

$$\text{Soluble lignin } (\%) = 100 \times \frac{A}{110} \times \frac{\text{Dilution}}{m_0}, \qquad (2)$$

where A is the absorbance at 280 nm, 110 is the absorptivity of soluble lignin measured in L/g/cm, m_0 (g) is the mass of CH.

The total lignin content in CH was calculated by the sum of insoluble lignin and soluble lignin according to the formula (3):

$$\text{Total lignin (\%)} = \text{Insoluble lignin (\%)} + \text{Soluble lignin (\%)}. \quad (3)$$

The experiment was repeated three times, and the lignin content was presented as mean ± SE.

Determination of caffeine content (59): 50 mg of ground CH was added to 100 mL of deionized water, the mixture was stirred and heated at 90°C for 30 min. The mixture was filtered into a 100 mL volumetric flask and made up to the mark with deionized water. 25 mL of the filtrate was extracted with 25 mL of dichloromethane and the absorbance was measured on a UV-Vis V630 spectroscopy (Jasco, Japan) at a wavelength of 275 nm. The experiment was repeated three times, using caffeine as the standard for the standard curve, the caffeine content was presented as mean ± SE and calculated according to the formula (4):

$$\text{Caffeine content (\%, } w/w) = 100 \times \frac{\text{Mass of caffeine (mg)}}{\text{Mass of CH (mg)}}. \quad (4)$$

Determination of cellulose and hemicellulose contents (60, 61)**:** 2.5 g of CH was extracted three times in 12.5 mL of hexane, dried to remove the solvent, and 80 mL of deionized water at 80°C was added to the remaining solid. The resulting suspension was treated with 1 g of $NaClO_2$ and 0.5 mL of acetic acid at 80°C for 4 h, then filtered, washed with deionized water, dried at 80°C for 24 h to constant weight, and the holocellulose (including cellulose and hemicellulose) was weighed. The holocellulose sample was treated twice with 100 mL of 17.5% NaOH for 30 min. The mixture was filtered, cleaned with deionized water, dried at 80°C for 24 h, and the cellulose was weighed. The hemicellulose content was calculated from the difference between the holocellulose and cellulose contents. The experiment was repeated three times, and the cellulose and hemicellulose content (%, w/w) were presented as mean ± SE.

Preparation of the Cu/Cu_2O/CH nanocomposite: 88 g of ground CH was moistened with 30 mL of deionized water. 20 mL solution containing 12 g of $CuSO_4.5H_2O$ was mixed well into moistened CH for 5 min, and the pH of the mixture was adjusted to ~9 with 2% NaOH solution. The mixture was left at room temperature for 30 min. to reduce Cu^{2+} ions. Then the mixture was dried at 105°C for 30 min to obtain the Cu/Cu_2O/CH nanocomposite.

Determination of properties of the **Cu/Cu_2O/CH nanocomposite:** Nanoparticle size was determined by scanning electron microscope (SEM) image measured on S-4800 (Hitachi – Japan), using ImageJ 1.54 g software. Elemental composition was determined by energy dispersive X-ray (EDX) on S-4800 (Hitachi – Japan) (61). The Cu content was determined by atomic absorption spectroscopy (AAS) on an AA-7000 (Shimadzu, Japan) according to OAOC 965.09, using C_2H_2 flame and measured at 324.7 nm. The crystallinity was determined by X-ray diffraction (XRD) spectroscopy on a D8 Advance X-ray diffractometer (Bruker, Germany), using Cu kα (λ = 1.5406 Å) radiation at 40 kV and 40 mA, 2θ diffraction angle from 5° to 80°. The crystalline size was calculated based on typical diffraction peaks in the XRD pattern by using Debye – Scherrer's equation: $d = k\lambda/\beta\cos\theta$ where d (nm) is the crystallite size, λ (CuKα wavelength, λ = 1.5406 Å) is the X-ray wavelength, β is the full width at half maximum (FWHM) of the peak in radian, θ is the X-rays incident angle in degree and k is the Scherrer constant that is close to unity (62). The bond characterization was determined by Fourier-transform infrared (FTIR) spectroscopy on an FTIR 8400S spectrometer (Shimadzu, Japan) in the wavenumber range of 4000–400 cm^{-1}.

Antifungal activity *in vitro* (63): The *P. capsici* fungus was inoculated into the center of a petri dish (90 mm) containing PDA medium diffused with the Cu/Cu_2O/CH nanocomposite at concentrations of 25, 35, 45, 55 mg/L Cu. The same petri dish contained CH at concentrations of 833, 1166, 1500, and 1833 mg/L (equivalent to the CH concentrations in the above nanocomposite samples). The control treatment did not diffuse the materials. After the fungus in the control treatment had covered the dish, the diameter of the fungal colony of the treated treatment was measured, and the diameter of the fungal colony was determined as the average of two perpendicular diagonals. The experiment was repeated three times, and the antifungal efficiency (AE) of the materials was presented as mean ± SE and calculated according to the formula (5):

$$AE(\%) = 100 \times \frac{D - d}{D}, \quad (5)$$

where D (mm) and d (mm) are the diameters of the fungal colony in the control and treated samples, respectively.

Germination experiment *in vitro* (64)**:** 15 mung bean seeds sterilized with NaClO were placed in a petri dish (10 cm) lined with filter paper, then 20 mL of the filtrate containing the Cu/Cu_2O/CH nanocomposite at a concentration of 100 mg/L Cu, and CH at a concentration of

3333 mg/L, the control treatment used deionized water. The petri dishes were incubated in the dark for 72 h, then the number of germinated mung bean seeds was counted and the root length was measured with an electronic caliper. The experiment was repeated three times, and the germination index (GI) was presented as the mean ± SE according to formula (6):

$$GI(\%) = 100 \times \frac{G \times L}{G_0 \times L_0}, \quad (6)$$

where G and G_0 are the average number of germinated seeds in the treated and control treatments, respectively. L and L_0 (cm) are the average length of roots in the treated and control treatments, respectively. GI > 80–100% means that the material is no longer phytotoxic and can be used to fertilize plants; GI > 100% means that the material can stimulate germination.

Statistical analysis: The particle size was measured by ImageJ 1.54 g. The results of *in vitro* experiment are presented as mean ± standard error (SE). All data were statistically processed using IRRISTAT 5.0 software and Microsoft Excel 2013. The means were compared using the least significant difference at 0.05 probability level ($LSD_{0.05}$). The inhibitory concentration 50% (IC_{50}) value is determined by replacing y = 50 and calculating x from the regression equation.

3. Results and discussion

The results of TP, RS, lignin, cellulose, hemicellulose, and caffeine content in CH are presented in Table 1.

TP content was calculated by the regression equation: y = 0.0520x – 0.0186 (R^2 = 0.9947), where x is absorbance and y is GA content (10–30 mg/L). RS content was calculated by the regression equation: y = 0.1799x + 0.0108 (R^2 = 0.9956), where x is absorbance and y is D-glucose content (100–250 mg/L). Caffeine content was calculated by the regression equation: y = 1.0067x – 0.0105 (R^2 = 0.9996), where x is absorbance and y is caffeine content (10–50 mg/L). The result of TP content in CH was 87.92 mg GAE/g, close to the result of Prihadi et al. (2020) of 10.5% (8), but much smaller than the result of Neves et al. (2019) of 184.79–382.97 mg GAE/g (9) and Boadu et al. (2023) of 354.3 mg GAE/g (65). The RS content in CH was determined to be 83.42 mg GE/g, which was lower than that of sticky CH in the study of Gouvea et al. (4). The above results showed that CH was mainly composed of cellulose 27.78%, lignin 9.17%, hemicellulose 3.98%, and caffeine 1.13%. The caffeine content in CH of this study was consistent with the result of 1.1% reported by Tello et al. (66). According to Gouvea et al. (4), the chemical composition of CH depended not only on the variety but also on the cultivation conditions.

Table 1. Chemical composition of CH.

Components	Content
TP (mg GAE/g)	87.92
RS (mg GE/g)	83.42
Lignin (%)d	9.17
Cellulose (%)	27.78
Hemicellulose (%)	3.98
Caffeine (%)	1.13

SEM images of CH and the Cu/Cu_2O/CH nanocomposite are presented in Figure 1. SEM images of CH in Figure 1a showed that CH had a rough typical cellulose crystal surface similar to the study of Nguyen et al. (2023) (61) and Gebresemati et al. (67). The width of cellulose crystals in CH was in the range of 0.5–4 µm, the length could not be determined by these SEM images, but according to Collazo-Bigliardi et al. (2018), the length of cellulose crystals in CH treated with alkali is in the range of 110–600 µm (68). SEM images of the Cu/Cu_2O/CH nanocomposite in Figure 1b showed that Cu and Cu_2O nanoparticles had an average size of 54.6 ± 28.2 nm, distributed in the range of 15.6–146.2 nm. Thus, the reaction between $CuSO_4$ and reducing agents in CH has formed Cu-based nanoparticles dispersed and stabilized on the surface of CH.

The XRD patterns of CH and the Cu/Cu_2O/CH nanocomposite are shown in Figure 2. The XRD pattern of CH in Figure 2a showed the characteristic peaks assigned to the cellulose crystal structure, including a low-intensity peak at 2θ ~15.02° and a broad peak with higher intensity at 2θ ~22.50°, corresponding to the diffraction planes (110) and (200). This result was consistent with other studies on CH (69, 70). In addition, the XRD pattern of CH also had a peak at 2θ ~22° which was considered to be the diffraction peak of amorphous silica (71, 72). The peaks in the XRD pattern of the Cu/Cu_2O/CH nanocomposite in Figure 2b included characteristic peaks of Cu and Cu_2O nanoparticles. The characteristic peaks of Cu nanoparticles were consistent with the data of JCPDS No. 040836 at 2θ ~44.28°, 50.40°, and 74.81° corresponding to the diffraction planes (111), (200), and (222) (73, 74). The characteristic peaks for Cu_2O nanoparticles at 2θ ~29.60, 36.52, 42.44, 61.54, and 73.69 correspond to the diffraction planes (110), (111), (200), (220), and (311) of Cu_2O crystals (73, 75), this result was consistent with the data of JCPDS No. 050667.

The average crystallite size of Cu and Cu_2O nanoparticles calculated from the Scherrer equation are presented in Table 2. The results in Table 2 showed that the average crystallite size of Cu and Cu_2O nanoparticles calculated at the characteristic highest diffraction peaks was 16.4 nm, which was smaller than the actual size of nanoparticles determined from SEM

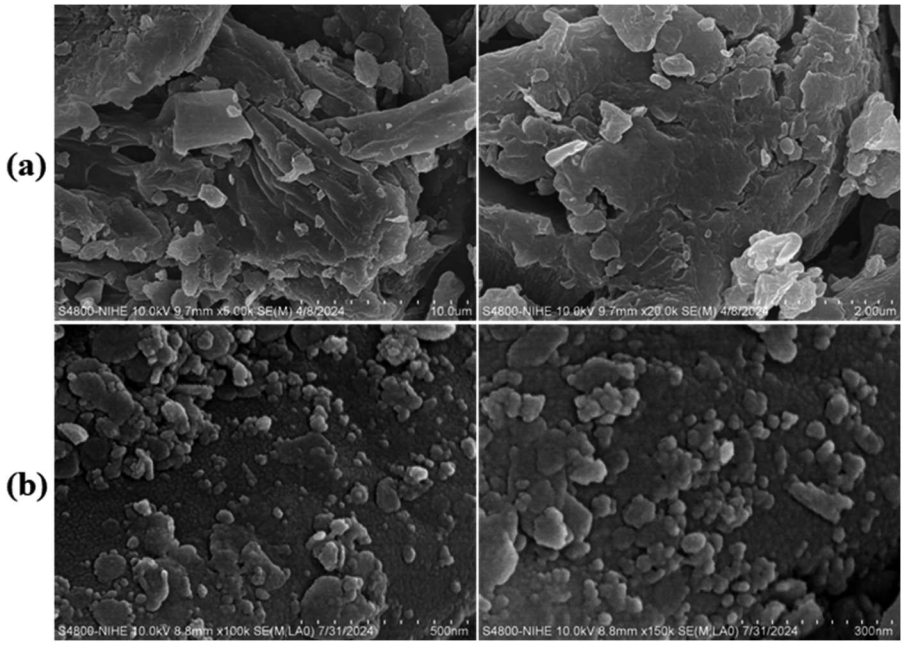

Figure 1. SEM images of CH (a) and the Cu/Cu_2O/CH nanocomposite (b).

images. Previously, Yan et al. (76) determined the size of Au nanoparticles from transmission electron microscopy (TEM) images, and the results were also larger than those calculated from the XRD pattern. The author assumed that particles with sizes > 50 nm had more than one crystal that could not be determined by the Scherrer equation (76). The results in this study were also similar to those of Pabisch et al. (77) when determining the size of ZrO_2 and SiO_2 particles using XRD patterns, TEM images, and other methods. Jensen et al. (78) also assumed that the Scherrer equation only determined the size of crystals, so there was a difference between it and the method of determining particle size using TEM and SEM images or small-angle X-ray scattering.

Thus, $CuSO_4$ was reduced by the reducing agents in CH (including RS and polyphenol) to a mixture of Cu_2O and Cu nanoparticles at alkaline pH. The mechanism of reduction of Cu^{2+} ions to Cu^{+} and Cu by RS, for example, glucose, according to Equations (7) and (8)

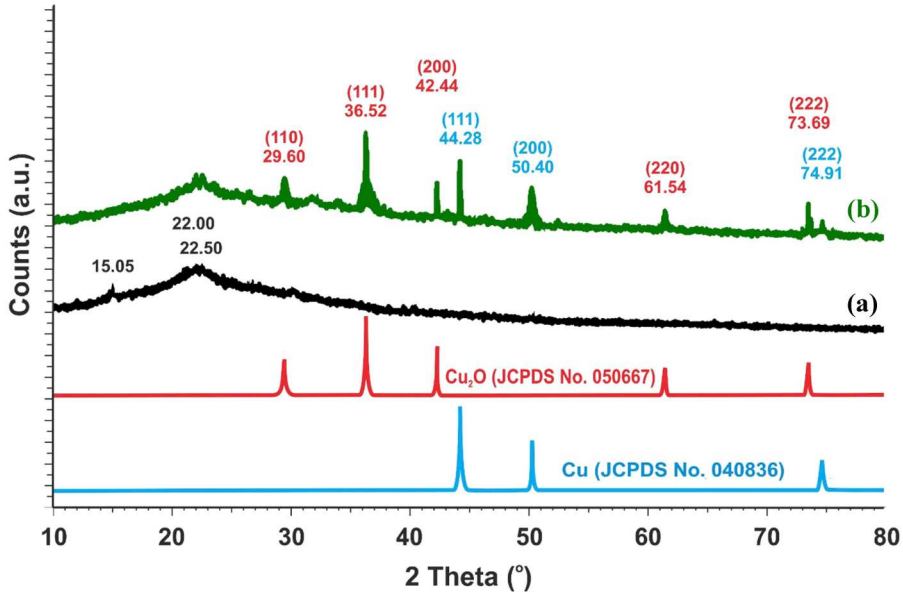

Figure 2. XRD pattern of CH (a) and the Cu/Cu_2O/CH nanocomposite (b).

Table 2. The nanoparticle size was estimated from the XRD pattern by using the Scherrer equation.

Nanoparticles	2θ (°)	hkl	β (°)	Crystallite size (nm)	Average crystal size
Cu	44.28	111	0.51813	17.3	16.4
Cu_2O	36.52	111	0.56442	15.5	

(79, 80):

$$Cu^{2+} + 3OH^- + C_6H_{12}O_6 \rightarrow Cu^+ + C_6H_{11}O_7^- + 2H_2O, \quad (7)$$

$$Cu^+ + OH^- \rightarrow CuOH, \quad (8)$$

$$2CuOH \rightarrow Cu_2O + H_2O, \quad (9)$$

$$CuSO_4.5H_2O + 2NaOH \rightarrow Cu(OH)_2 + Na_2SO_4 + 5H_2O, \quad (10)$$

$$Cu(OH)_2 \rightarrow CuO + H_2O, \quad (11)$$

$$10C_6H_{12}O_6 + 120CuO \rightarrow 120Cu + 60CO_2 + 603H_2O. \quad (12)$$

In the case of polyphenols reacting with Cu^{2+}, based on the chemical point of view, polyphenols easily donate an electron or hydrogen atom to the oxidant or free radical to form a less stable (more active) free radical (81, 82). The reduction reaction mechanism of polyphenols with Cu^{2+} according to Equations (9)–(11) (83, 84), and resultant Cu^+ ions in an alkaline environment combined with heating will form Cu_2O nanoparticles according to reactions (8) and (9) above.

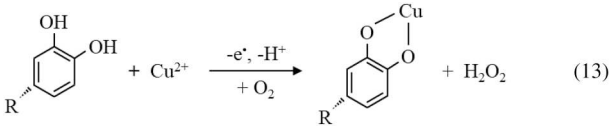

(13)

$$Cu^{2+} + H_2O_2 \rightarrow Cu^+ + O_2^-, \quad (14)$$

$$O_2^- + H_2O \rightarrow H_2O_2. \quad (15)$$

The EDX spectra scanned from the SEM images with an area of 1 μm^2 and elemental compostion of CH and the Cu/Cu_2O/CH nanocomposites are presented in Figure 3 and Table 3. The results showed that the composition of CH in Figure 3a mainly consisted of C 57.22%, and O 39.92%, which were the elements that made up cellulose, hemicellulose, lignin, and other organic substances. In addition, CH also contained some minerals such as Mg 0.15%, Al 0.23%, Si 0.66%, S 0.26%, K 1.07%, and Ca 0.49%, this result was similar to the study of Nguyen et al. (2023) on the composition of Robusta CH in Vietnam (61). The EDX spectrum of the Cu/Cu_2O/CH nanocomposite in Figure 3b showed that, in addition to the elements present in CH, the nanocomposite also contained approximately 2.98% C. The elemental map of the nanocomposite in Table 3 confirmed that Cu and Cu_2O nanoparticles were uniformly dispersed in CH. In addition, the Cu content determined by the AAS method was 31.49 g/kg (~3.15%).

The FTIR spectra of CH and the Cu/Cu_2O/CH nanocomposite are presented in Figure 4. The FTIR spectrum of CH in Figure 4a showed the characteristic peaks for bond vibrations. Specifically, the peak at 3441 cm^{-1} was assigned to the stretching vibration of the O–H bond present in phenolics, alcohols, carboxylic acids, and other hydroxyl-containing compounds (85). The peak at 2926 cm^{-1} was assigned to the C–H symmetric vibration of hemicellulose and lignin (61, 85). The low-intensity peak at 1734cm^{-1} represented the stretching vibration of the C = O bond in aldehydes, and ketones (86). The peak at 1628 cm^{-1} was the C=C stretching vibration of hemicellulose and lignin. The peak at 1600 cm^{-1} had a strong intensity, related to the C=C bond of the aromatic group in lignin (87), the two peaks at 1512, 1401 cm^{-1} were related to the vibration of aromatic rings and C–H bonds of organic molecules (88), and the peak at 1095 cm^{-1} typical for Si–O–Si group (89, 90).

The FTIR spectrum of the Cu/Cu_2O/CH nanocomposite in Figure 4b showed all the characteristic peaks of CH, and there was an additional peak at 618 cm^{-1}, which was characteristic of the Cu–O bond of the Cu_2O molecule (91–93). In addition, the characteristic peaks for the O–H bond stretching at 3441 cm^{-1} shifted to 3434 cm^{-1}. Thus, there was an electrostatic interaction between the hydroxyl groups in CH with the charged Cu and Cu_2O particles reducing the intramolecular hydrogen bonding. Notably, the FTIR spectrum of the Cu/Cu_2O/CH nanocomposite did not show the peak at 1734cm^{-1}, possibly because the aldehyde-reducing agent reacted with Cu^{2+} ions. Therefore, the Cu and Cu_2O nanoparticles interacted electrostatically with the hydroxyl groups of the lignocellulose and hemicellulose in CH.

The caffeine content in the Cu/Cu_2O/CH nanocomposite was determined to be 0.05% (w/w) compared to that of 1.13% (w/w) in CH. Thus, the caffeine removal efficiency after forming the Cu/Cu_2O/CH nanocomposite was ~95.6%. Recently, nanomaterials have been studied for use as photocatalysts to decompose caffeine in wastewater. Fe/Cu nanoparticles bimetallic were able to remove caffeine with an efficiency of 86% (46). Cu nanoparticles attached to graphite carbon nitride were able to remove 88% caffeine (94). CuO nanoparticles impregnated on activated carbon were able to decompose ~99% of caffeine-contaminated wastewater (45).

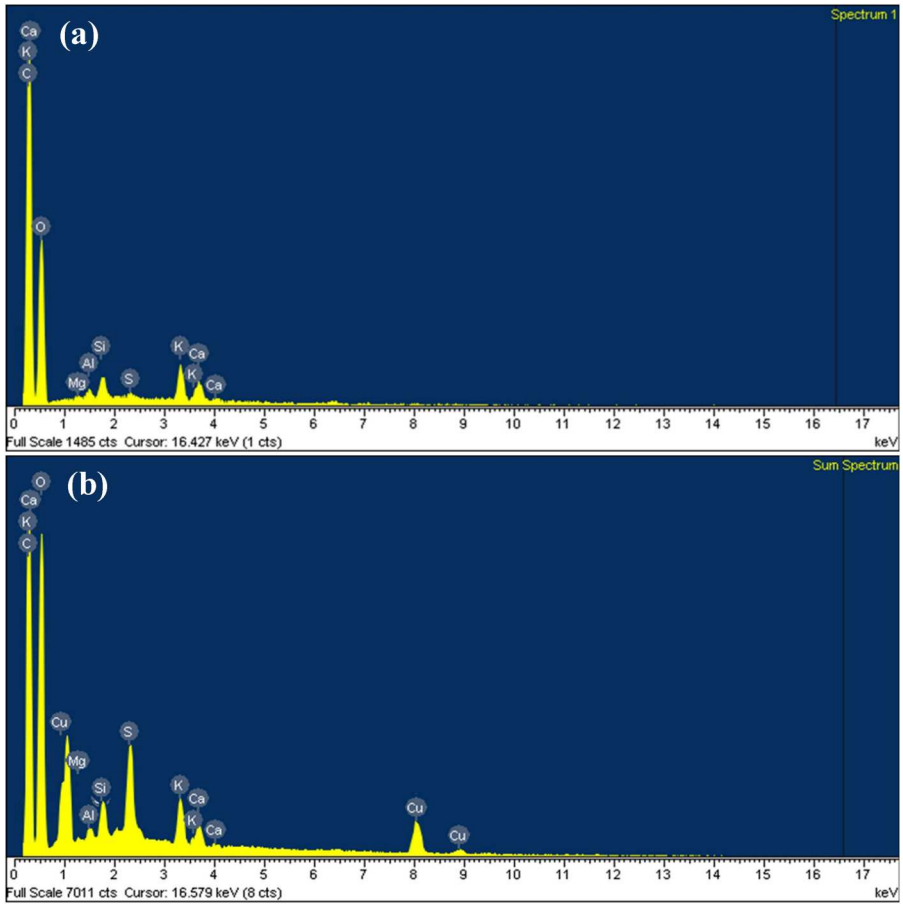

Figure 3. EDX spectra of CH (a) and the Cu/Cu_2O/CH nanocomposite (b).

Similarly, photocatalytic nanoparticles such as TiO_2, $AgFeO_2$, and ZnO also had high caffeine decomposition efficiency (47, 95, 96). Thakur et al. (2021) proposed that the mechanism of caffeine degradation of ZnO nanoparticles is due to the production of reactive oxygen species (ROS) such as $O_2^{\bullet -}$, $^{\bullet}OH$ which decompose caffeine into CO_2 and H_2O under solar light (47), and Cu and Cu@Cu_2O nanoparticles also generated ROS by the same mechanism (97).

In general, Cu, Ag, and Fe nanoparticles can be considered to have a Fenton-like mechanism of organic compound degradation because they have a lower redox potential than the redox couple of H_2O_2/H_2O (1.77 V vs. NHE) (98). Cu_2O nanoparticles are a p-type semiconductor with a small band gap energy of 2.1–2.17 V and operate in the visible light region (99, 100), so it is effective in catalyzing the decomposition of caffeine and some other organic pollutants. The study results demonstrated that the Cu/Cu_2O/CH nanocomposite containing 3% Cu, achieved high efficiency in caffeine decomposition when dried at a temperature of 105°C. The obtained the Cu/Cu_2O/CH nanocomposite can be simultaneously used as a plant-disease control agent and micronutrient fertilizer due to its low caffeine content that is non-toxic for plants.

Table 3. Average elemental composition of CH and the Cu/Cu_2O/CH nanocomposite.

	Weight (%)	
Element	CH	Cu/Cu_2O/CH
C K	57.22	52.77
O K	39.92	40.07
Mg K	0.15	0.13
Al K	0.23	0.20
Si K	0.66	0.60
S K	0.26	1.74
K K	1.07	1.05
Ca K	0.49	0.46
Cu K	–	2.98

The *in vitro* antifungal activity results of CH and the Cu/Cu_2O/CH nanocomposite are shown in Figure 5 and Table 4. Figure 5a showed that the fungal colony in the control treatment filled the petri dish after 7 days of incubation. The antifungal activity of materials in Table 4 indicated that the CH diffusion treatment at concentrations of 833 and 1167 mg/L did not show any antifungal activity, while at higher concentrations of 1500 and 1833 mg/L, the antifungal activity was low at 10.89% and 14.78%, respectively. As is known, polyphenols have antibacterial activity against both gram-

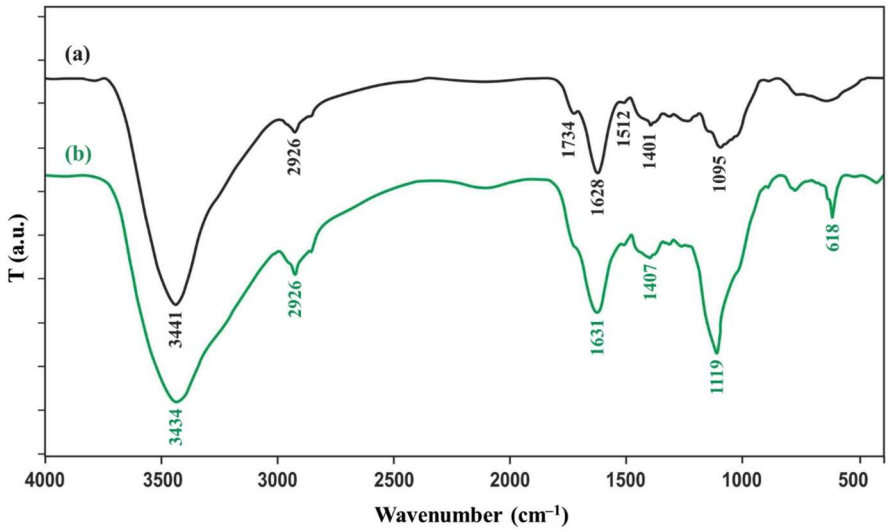

Figure 4. The FTIR spectra of CH (a) and the Cu/Cu_2O/CH nanocomposite (b).

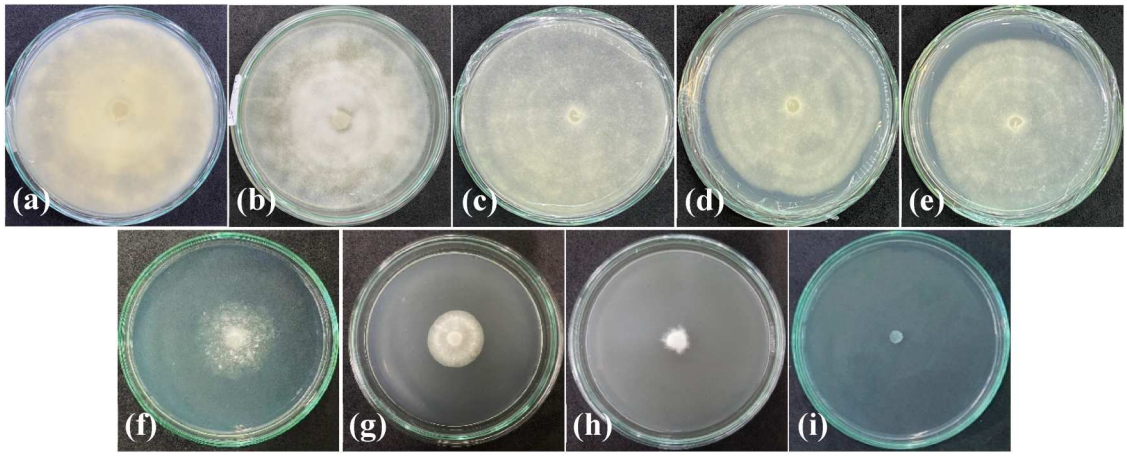

Figure 5. Growth of *P. capsici* in the experimental treatments after 7 days incubation: Control (a); CH at concentrations of 833 mg/L (b), 1167 mg/L (c), 1500 mg/L (d), 1833 mg/L (e); Cu/Cu_2O/CH at Cu concentrations of 25 mg/L (f), 35 mg/L (g), 45 mg/L (h), and 55 mg/L (i).

positive and gram-negative bacteria (101, 102). In addition, polyphenols also showed the ability to inhibit some fungi such as *Candida famata*, *Candida utilis*, *Candida albicans*, *Saccharomyces cerevisiae*, and *Candida neoformans* (103, 104). However, the CH containing polyphenols used in this study also exhibited *P. capsici* but at low efficiency. For the Cu/Cu_2O/CH nanocomposite, the AE against *P. capsici* increased proportionally with Cu concentration. Specifically, in the diffusion treatments of the Cu/Cu_2O/CH nanocomposite with concentrations of 25 and 35 mg/L Cu, the AE was relatively high at 58.22% and 65.33%, respectively. When the Cu concentration was increased to 45 and 55 mg/L, the AE reached 85.22 and 93.52%, respectively. Thus, the Cu/Cu_2O/CH nanocomposite effectively resisted *P. capsici* at a concentration of 55 mg/L Cu, almost completely inhibiting fungal growth.

Table 4. The antifungal activity of the Cu/Cu_2O/CH nanocomposite against *P. capsici in vitro*.

Material	Diameter (cm)	Inhibitory effect (%)
Control	$9.00^a \pm 0.00$	–
CH 833 mg/L	$9.00^a \pm 0.00$	0.00
CH 1167 mg/L	$9.00^a \pm 0.00$	0.00
CH 1500 mg/L	$8.02^b \pm 0.34$	10.93
CH 1833 mg/L	$7.67^b \pm 0.39$	14.81
Cu/Cu_2O/CH (25 mg/L Cu)	$3.76^c \pm 0.34$	58.22
Cu/Cu_2O/CH (35 mg/L Cu)	$3.12^d \pm 0.08$	65.33
Cu/Cu_2O/CH (45 mg/L Cu)	$1.33^e \pm 0.17$	85.22
Cu/Cu_2O/CH (55 mg/L Cu)	$0.58^f \pm 0.21$	93.52
$LSD_{0,05}$	0.48	–

Note: The mean values in a column with the same letter are not significantly different at $P < 0.05$.

Based on the results in Table 4, the regression equation of the correlation between AE and Cu

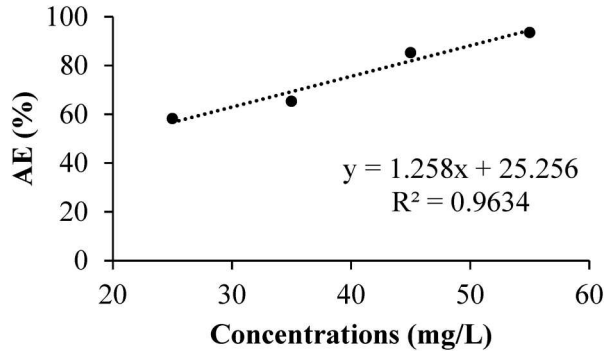

Figure 6. The relationship of Cu concentrations and AE against *P. capsici* of the Cu/Cu_2O/CH nanocomposite.

Table 5. Effects of materials on growth and germination of mung bean seeds.

Materials	Average root length (cm)	G (seeds)	GI (%)
Control	2.98 ± 0.31	12.00^{ab} ± 0.58	100.00
CH (3333 mg/L)	1.85 ± 0.54	10.67^{b} ± 0.88	55.12
Cu/Cu_2O/CH (100 mg/L Cu)	2.79 ± 0.41	13.33^{a} ± 0.33	103.79
$LSD_{0,05}$	1.99^{ns}	2.92	–

Note: The mean values in a column with the same letter are not significantly different at $P < 0.05$.

concentration of nanocomposite was inferred as: y = 1.258x + 25.256 (Figure 6). The IC_{50} value of the Cu/Cu_2O/CH nanocomposite against *P. capsici* calculated from this equation was 19.67 mg/L Cu.

Previously, many authors have studied the use of Cu and Cu oxide nanoparticles against *P. capsici*, *P. nicotianae*, *P. parasitica*, the effective concentration of these nanoparticles was 30–150 ppm (105–107). Guerrero et al. (2020) tested commercial CuO nanoparticles against *P. capsici* and the results showed that the AE reached 100% after 07 days at concentrations of 500–1500 ppm, however, the author did not investigate at lower concentrations (108). It is clearly evident that the Cu/Cu_2O/CH nanocomposite in this study effectively inhibited the *P. capsici* at concentrations below 100 mg/L. Therefore, the Cu/Cu_2O/CH nanocomposite has the potential for use as a plant-disease control agent in soil environments because Cu concentrations below 100 mg/kg soil did not affect soil properties and microbial populations (109, 110). Similarly, Kumar et al. (2021) (111) reported that applying Cu at concentrations of 2-109 mg/kg did not have a negative impact on agricultural land. In the soil environment, Cu NPs were converted into Cu^{2+} ions, and the survival time of Cu NPs depended on particle size, humidity, pH, and organic content in the soil (15). Furthermore, Cu is one of the essential micronutrients necessary for the growth and development of plants, as it is involved in many important biological and physiological processes in plants (112). Therefore, applying the Cu/Cu_2O/CH nanocomposite to plants for soil-borne disease management will allow the plants to consume Cu compounds, subsequently reducing Cu accumulation in the soil.

The *in vitro* germination results of mung beans treated with CH and the Cu/Cu_2O/CH nanocomposite are shown in Table 5 and Figure 7. The results in Table 5 show that in the control treatment using deionized water, the germination rate of mung bean seeds was 80%, and the average root length was 2.98 cm. For the treatment using CH, the germination rate and average root length all decreased by 71.13% and 1.85 cm, respectively. For the Cu/Cu_2O/CH nanocomposite treatment, the germination rate and average root length all decreased by 88.87% and 2.79 cm, respectively. Finally, the GI indexes were 100%, 55.12%, and 103.79% for the control, CH, and the Cu/Cu_2O/CH nanocomposite treatments, respectively. The results indicated that the direct use of CH containing caffeine and organic acids affected the germination and growth of plants as previously published studies (51–53). The use of the Cu/Cu_2O/CH nanocomposite to treat seeds to stimulate germination and plant growth has been studied, especially Cu, Fe, and Zn nanoparticles. Zhao et al. (113) reported that Cu, Fe, and Zn nanoparticles at low concentrations of 2×10^{-4} mM, 1.8×10^{-4} mM, and 4.6×10^{-5} mM,

Figure 7. Experiment on mung bean germination after 72 h in different treatments.

respectively, all had positive effects on germination and growth in tomato. Hien and Van (114) demonstrated that when maize seeds were treated with Cu nanoparticles at a concentration of 20 mg/kg, the germination index and growth parameters were higher than the control. However, the use of Cu nanoparticles at high concentrations of 200–1000 mg/L to treat seeds of *Phaseolus radiatus* L. and *Triticum aestivum* ssp. *aestivum* reduced the growth of seedlings after germination (115). Thus, the use of the Cu/Cu_2O/CH nanocomposite at a concentration of 100 mg/L Cu had the effect of stimulating germination and did not affect the growth and development of mung beans.

4. Conclusion

In this study, a green chemistry method was used to synthesize Cu-based nanoparticles using CH as a reductant and stabilizer. The synthesis of the Cu/Cu_2O/CH nanocomposite is favorable for large-scale production. Furthermore, the synthesized Cu/Cu_2O/CH nanocomposite with a high Cu content of ~3% exhibited highly antifungal activity against *P. capsici* with an IC_{50} of 19.68 mg/L Cu *in vitro* experiment. At a concentration of 100 mg/L Cu, the Cu/Cu_2O/CH nanocomposite did not show any phytotoxicity in the mung bean germination. Therefore, the obtained Cu/Cu_2O/CH nanocomposite has the potential to be used as a plant-disease control agent and a micronutrient fertilizer for plant growth.

Acknowledgments

This research is funded by Vietnam National Foundation for Science and Technology Development (NAFOSTED) under grant number NCUD.02-2023.28.

Disclosure statement

No potential conflict of interest was reported by the author(s).

References

[1] Mard.gov.vn. Vietnam's coffee exports doubled in January 2024, 17 02 2024. https://mard.gov.vn/en/Pages/vietnam-s-coffee-exports-doubled-in-january-2024.aspx. [Accessed 19 08 2024].

[2] Flammini, A.; Brundin, E.; Grill, R.; Zellweger, H. Supply Chain Uncertainties of Small-Scale Coffee Husk-Biochar Production for Activated Carbon in Vietnam. *Sustainability* **8069,** *12* (19), 2020.

[3] Pérez, J.M.; Pulgarín, J.A.; Loaiza, M.A.; Restrepo, E.M.; Quintero, G.P.; Tascón, C.O. Propiedades Físicas y Factores de Conversión del Café en el Proceso de Beneficio. *Avances Técnicos Cenicafé* **2008,** *370*.

[4] Gouvea, B.M.; Torres, C.; Franca, A.S.; Oliveira, L.S.; Oliveira, E.S. Feasibility of Ethanol Production from Coffee Husks. *Biotechnol. Lett.* **2009,** *31* (9), 1315–1319. doi:10.1007/s10529-009-0023-4.

[5] Toscano, S.; Trivellini, A.; Cocetta, G.; Bulgari, R.; Francini, A.; Romano, D.; Ferrante, A. Effect of Preharvest Abiotic Stresses on the Accumulation of Bioactive Compounds in Horticultural Produce. *Front. Plant Sci.* **2019**, *10*, 1212.

[6] Francini, A.; Pintado, M.; Manganaris, G.A.; Ferrante, A. Bioactive Compounds Biosynthesis and Metabolism in Fruit and Vegetables. *Front. Plant Sci.* **2020 ,** *11*, 129.

[7] Adams, M.R.; Dougan, J. *Waste Products, in Coffee Volume 2: Technology*; Springer: Dordrecht, **1987**, , 257–291.

[8] Prihadi, A.R.; Maimulyanti, A.; Mellisani, B.; Nurhasanah, N. Antioxidant Activity, Tannin Content and Dietary Fiber from Coffee Husk Extract and Potential for Nutraceutical. *Rasayan Journal of Chemistry* **2020,** *13* (2), 955–959. doi:10.31788/RJC.2020.1325613.

[9] Neves, J.V.G.D.; Borges, M.V.; Silva, D.D.M.; Leite, C.X.D.S.; Santos, M.R.C.; Lima, N.G.B.D.; Lannes, S.C.S.; Silva, M.V.D. Total Phenolic Content and Primary Antioxidant Capacity of Aqueous Extracts of Coffee Husk: Chemical Evaluation and Beverage Development. *Food Sci. Technol.* **2019,** *39*, 348–353. doi:10.1590/fst.36018.

[10] Silva, M.D.O.; Honfoga, J.N.B.; Medeiros, L.L.D.; Madruga, M.S.; Bezerra, T.K.A. Obtaining Bioactive Compounds from the Coffee Husk (*Coffea Arabica* L.) Using Different Extraction Methods. *Molecules* **2020**, *26* (1), 46.

[11] Pham, T.T.H.; Tran, T.T.T. Research on Factors Affecting the Extractability of Antioxidant Compounds from Coffee Husks Abstract. *VNUHCM J. Eng. Technol.* **2020,** *3* (1), 375–382.

[12] Terra, S.; Melengati, J.; Rosado, C.P.; Alves, E.A.; Rocha, R.B.; Teixeira, A.; Teodoro, A.J.. Antioxidant activity and total phenolic content of amazonian robusta coffee husk: The influence of self-induced anaerobiosis fermentation, In Anais do 15° SLACAN - Simpósio Latino Americano de Ciência de Alimentos e Nutrição, Campinas, 2023.

[13] Febrianto, N.A.; Zhu, F. Coffee Bean Processing: Emerging Methods and Their Effects on Chemical, Biological and Sensory Properties. *Food Chem.* **2023,** *412*, 135489.

[14] Su, C.; Chen, A.; Liang, W.; Xie, W.; Xu, X.; Zhan, X.; Zhang, W.; Peng, C. Copper-based Nanomaterials: Opportunities for Sustainable Agriculture. *Sci. Total Environ.* **2024,** *926*, 171948.

[15] Bakshi, M.; Kumar, A. Copper-based Nanoparticles in the Soil-Plant Environment: Assessing Their Applications, Interactions, Fate and Toxicity. *Chemosphere* **2021,** *281*, 130940.

[16] Elmer, W.; Ma, C.; White, J. Nanoparticles for Plant Disease Management. *Curr. Opin. Environ., Sci. Health* **2018,** *6*, 66–70. doi:10.1016/j.coesh.2018.08.002.

[17] Ballabio, C.; Panagos, P.; Lugato, E.; Huang, J.H.; Orgiazzi, A.; Jones, A.; Fernández-Ugalde, O.; Borrelli, P.; Montanarella, L. Copper Distribution in European Topsoils: An Assessment Based on LUCAS Soil Survey. *Sci. Total Environ.* **2018,** *636*, 282–298. doi:10.1016/j.scitotenv.2018.04.268.

[18] Liu, Y.; Zhao, W.; Yin, Y.; Adeel, M.; Shakoor, N.; Li, Y.; Tan, Z.; Rui, Y.; Zhang, Q.; Liu, J., et al. Agricultural

Applications and Potential Risks of Copper-Based Nanoagrochemicals in Crop Cultivation. *Rev. Environ. Contam. Toxicol.* **2022,** *260*, 20.n

[19] Rai, M.; Ingle, A.P.; Pandit, R.; Paralikar, P.; Shende, S.; Gupta, I.; Biswas, J.K.; da Silva, S.S. Copper and Copper Nanoparticles: Role in Management of Insect-Pests and Pathogenic Microbes. *Nanotechnol. Rev.* **2018,** *7* (4), 303–315. doi:10.1515/ntrev-2018-0031.

[20] Ibrahim, A.S.; Ali, G.A.; Hassanein, A.; Attia, A.M.; Marzouk, E.R. Toxicity and Uptake of CuO Nanoparticles: Evaluation of an Emerging Nanofertilizer on Wheat (*Triticum Aestivum* L.) Plant. *Sustainability* **4914,** *14* (9), 2022.

[21] Giannousi, K.; Avramidis, I.; Dendrinou-Samara, C. Synthesis, Characterization and Evaluation of Copper Based Nanoparticles as Agrochemicals Against *Phytophthora Infestans*. *RSC Adv.* **2013,** *3* (44), 21743–21752. doi:10.1039/c3ra42118j.

[22] Mondal, K.K.; Mani, C. Investigation of the Antibacterial Properties of Nanocopper Against *Xanthomonas Axonopodis* pv. *Punicae*, the Incitant of Pomegranate Bacterial Blight. *Ann. Microbiol.* **2012,** *62*, 889–893. doi:10.1007/s13213-011-0382-7.

[23] Brunel, F.; El Gueddari, N.E.; Moerschbacher, B.M. Complexation of Copper (II) with Chitosan Nanogels: Toward Control of Microbial Growth. *Carbohydr. Polym.* **2013,** *92* (2), 1348–1356. doi:10.1016/j.carbpol.2012.10.025.

[24] Kanhed, P.; Birla, S.; Gaikwad, S.; Gade, A.; Seabra, A.B.; Rubilar, O.; Duran, N.; Rai, M. *In Vitro* Antifungal Efficacy of Copper Nanoparticles Against Selected Crop Pathogenic Fungi. *Mater. Lett.* **2014,** *115*, 13–17. doi:10.1016/j.matlet.2013.10.011.

[25] Bramhanwade, K.; Shende, S.; Bonde, S.; Gade, A.; Rai, M. Fungicidal Activity of Cu Nanoparticles Against *Fusarium* Causing Crop Diseases. *Environ. Chem. Lett.* **2016,** *14*, 229–235. doi:10.1007/s10311-015-0543-1.

[26] Ren, G.; Hu, D.; Cheng, E.W.; Vargas-Reus, M.A.; Reip, P.; Allaker, R.P. Characterisation of Copper Oxide Nanoparticles for Antimicrobial Applications. *Int. J. Antimicrob. Agents* **2009,** *33* (6), 587–590. doi:10.1016/j.ijantimicag.2008.12.004.

[27] Ingle, A.; Duran, N.; Rai, M. Bioactivity, Mechanism of Action, and Cytotoxicity of Copper-Based Nanoparticles: A Review. *Appl. Microbiol. Biotechnol.* **2014,** *98*, 1001–1009. doi:10.1007/s00253-013-5422-8.

[28] Lemire, J.A.; Harrison, J.J.; Turner, R.J. Antimicrobial Activity of Metals: Mechanisms, Molecular Targets and Applications. *Nat. Rev. Microbiol.* **2013,** *11*, 371–384. doi:10.1038/nrmicro3028.

[29] Swarnkar, R.K.; Pandey, J.K.; Soumya, K.K.; Dwivedi, P.; Sundaram, S.; Prasad, S.; Gopal, R. Enhanced Antibacterial Activity of Copper/Copper Oxide Nanowires Prepared by Pulsed Laser Ablation in Water Medium. *Appl. Phys. A* **2016,** *122*, 704.

[30] Biswas, A.; Bayer, I.S.; Biris, A.S.; Wang, T.; Dervishi, E.; Faupel, F. Advances in top-Down and Bottom-up Surface Nanofabrication: Techniques, Applications & Future Prospects. *Adv. Colloid Interface Sci.* **2012,** *170* (1/2), 2–27. doi:10.1016/j.cis.2011.11.001.

[31] Umer, A.; Naveed, S.; Ramzan, N.; Rafique, M.S. Selection of a Suitable Method for the Synthesis of Copper Nanoparticles. *Nano* **2012,** *7* (5), 1230005.

[32] Gawande, M.B.; Goswami, A.; Felpin, F.X.; Asefa, T.; Huang, X.; Silva, R.; Zou, X.; Zboril, R.; Varma, R.S. Cu and Cu-Based Nanoparticles: Synthesis and Applications in Catalysis. *Chem. Rev.* **2016,** *116* (6), 3722–3811. doi:10.1021/acs.chemrev.5b00482.

[33] Harish, V.; Ansari, M.M.; Tewari, D.; Gaur, M.; Yadav, A.B.; García-Betancourt, M.L.; Abdel-Haleem, F.M.; Bechelany, M.; Barhoum, A. Nanoparticle and Nanostructure Synthesis and Controlled Growth Methods. *Nanomaterials* **2022,** *12* (18), 3226.

[34] Mohamed, E.A. Green Synthesis of Copper & Copper Oxide Nanoparticles Using the Extract of Seedless Dates. *Heliyon* **2020,** *6*, e03123.

[35] Ramesh, C.; Hariprasad, M.; Ragunathan, V.; Jayakumar, N. A Novel Route for Synthesis and Characterization of Green Cu_2O/PVA Nano Composites. *Eur. J. Appl. Eng. Sci. Res.* **2012,** *1* (4), 201–206.

[36] Li, W.; Ai, S. Green and Gentle Synthesis of Cu_2O Nanoparticles Using Lignin as Reducing and Capping Reagent with Antibacterial Properties. *J. Exp. Nanosci.* **2016**, *11* (1), 18–27. doi:10.1080/17458080.2015.1015462.

[37] Leng, W.; Barnes, H.M.; Yan, Q.; Cai, Z.; Zhang, J. Low Temperature Synthesis of Graphene-Encapsulated Copper Nanoparticles from Kraft Lignin. *Mater. Lett.* **2016,** *185*, 131–134. doi:10.1016/j.matlet.2016.08.122.

[38] Nasar, M.Q.; Zohra, T.; Khalil, A.T.; Saqib, S.; Ayaz, M.; Ahmad, A.; Shinwari, Z.K. Seripheidium Quettense Mediated Green Synthesis of Biogenic Silver Nanoparticles and Their Theranostic Applications. *Green Chem. Lett. Rev.* **2019,** *12* (3), 310–322. doi:10.1080/17518253.2019.1643929.

[39] Khan, M.R.; Hoque, S.M.; Hossain, K.F.B.; Siddique, M.A.B.; Uddin, M.K.; Rahman, M.M. Green Synthesis of Silver Nanoparticles Using *Ipomoea Aquatica* Leaf Extract and its Cytotoxicity and Antibacterial Activity Assay. *Green Chem. Lett. Rev.* **2020,** *13* (4), 303–315. doi:10.1080/17518253.2020.1839573.

[40] Khan, A.; Mfarrej, M.F.B.; Danish, M.; Shariq, M.; Khan, M.F.; Ansari, M.S.; Hashem, M.; Alamri, S.; Ahmad, F. Synthesized Copper Oxide Nanoparticles via the Green Route act as Antagonists to Pathogenic Root-Knot Nematode, *Meloidogyne Incognita*. *Green Chem. Lett. Rev.* **2022,** *15* (3), 491–507. doi:10.1080/17518253.2022.2096416.

[41] Shah, A.T.; Ahmad, S.; Kashif, M.; Khan, M.F.; Shahzad, K.; Tabassum, S.; Mujahid, A. In Situ Synthesis of Copper Nanoparticles on SBA-16 Silica Spheres. *Arab. J. Chem.* **2016,** *9* (4), 537–541. doi:10.1016/j.arabjc.2014.02.013.

[42] Dong, Y.; Wang, K.; Tan, Y.; Wang, Q.; Li, J.; Mark, H.; Zhang, S. Synthesis and Characterization of Pure Copper Nanostructures Using Wood Inherent Architecture as a Natural Template. *Nanoscale Res. Lett.* **2018,** *13*, 119.

[43] Du, B.D.; Phu, D.V.; Quoc, L.A.; Hien, N.Q. Synthesis and Investigation of Antimicrobial Activity of Cu_2O Nanoparticles/Zeolite. *J. Nanopart.* **2017,** *1*, 7056864.

[44] Musa, A.; Ahmad, M.B.; Hussein, M.Z.; Izham, S.M.; Shameli, K.; Sani, H.A. Synthesis of Nanocrystalline Cellulose Stabilized Copper Nanoparticles. *J. Nanomater.* **2016,** *1*, 2490906.

[45] Peternela, J.; Silva, M.F.; Vieira, M.F.; Bergamasco, R.; Vieira, A.M.S. Synthesis and Impregnation of Copper

Oxide Nanoparticles on Activated Carbon Through Green Synthesis for Water Pollutant Removal. *Mater. Res.* **2017,** *21*, e20160460.
[46] Abdel-Aziz, H.M.; Farag, R.S.; Abdel-Gawad, S.A. Removal of Caffeine from Aqueous Solution by Green Approach Using *Ficus Benjamina* Zero-Valent Iron/Copper Nanoparticles. *Adsorp. Sci. Technol.* **2020,** *38* (9/10), 325–343. doi:10.1177/0263617420947495.
[47] Thakur, S.; Neogi, S.; Ray, A.K. Morphology-controlled Synthesis of ZnO Nanostructures for Caffeine Degradation and *Escherichia Coli* Inactivation in Water. *Catalysts* **2021**, *11* (1), 63.
[48] Andrade, M.B.; Santos, T.R.T.; Guerra, A.C.S.; Silva, M.F.; Demiti, G.M.M.; Bergamasco, R. Evaluation of Magnetic Nano Adsorbent Produced from Graphene Oxide with Iron and Cobalt Nanoparticles for Caffeine Removal from Aqueous Medium. *Chem. Eng. Process. Process Intensif.* **2022,** *170*, 108694.
[49] Ghosh, M.; Manoli, K.; Shen, X.; Wang, J.; Ray, A.K. Solar Photocatalytic Degradation of Caffeine with Titanium Dioxide and Zinc Oxide Nanoparticles. *J. Photochem. Photobiol. A* **2019,** *377*, 1–7. doi:10.1016/j.jphotochem.2019.03.029.
[50] Su, Q.; Zuo, C.; Liu, M.; Tai, X. A Review on Cu_2O-Based Composites in Photocatalysis: Synthesis,: Modification, and Applications. *Molecules* **2023,** *28* (14), 5576.
[51] Batish, D.R.; Singh, H.; Kaur, M.; Kohli, R.K.; Yadav, S.S. Caffeine Affects Adventitious Rooting and Causes Biochemical Changes in the Hypocotyl Cuttings of Mung Bean (*Phaseolus Aureus* Roxb). *Acta Physiol. Plant.* **2008,** *30*, 401–405. doi:10.1007/s11738-007-0132-4.
[52] Ferguson, S. Effects of caffeine and vitamin E on Wisconsin Fast Plant. *Best Integrated Writing*. **2015**, *2*, 2.
[53] Hanafi, N.N.M.; Azni, N.A.N.; Maraikan, H.H.J.; Mokhtar, W.N.F.A.W.; Azam, N.A.N.; Seman-Kamarulzaman, A.F. Studies on the Effect of Caffeine on the Growth Rate of Ipomoea Aquatic. *J. Sci. Technol.* **2020,** *3* (2), 20–25.
[54] Kitou, M.; Yoshida, S. Effect of Coffee Residue on the Growth of Several Crop Species. *J. Weed Sci. Technol.* **1997,** *42* (1), 25–30. doi:10.3719/weed.42.25.
[55] Geremu, M.; Tola, Y.B.; Sualeh, A. Extraction and Determination of Total Polyphenols and Antioxidant Capacity of red Coffee (*Coffea Arabica* L.) Pulp of wet Processing Plants. *Chem. Biol. Technol. Agric.* **2016,** *3*, 25.
[56] Khatri, D.; Chhetri, S.B.B. Reducing Sugar, Total Phenolic Content, and Antioxidant Potential of Nepalese Plants. *BioMed Res. Int.* **2020**, 7296859.
[57] Carrier, M.; Loppinet-Serani, A.; Denux, D.; Lasnier, J.M.; Ham-Pichavant, F.; Cansell, F.; Aymonier, C. Thermogravimetric Analysis as a new Method to Determine the Lignocellulosic Composition of Biomass. *Biomass Bioenergy* **2011,** *35* (1), 298–307. doi:10.1016/j.biombioe.2010.08.067.
[58] Galiwango, E.; Rahman, N.S.A.; Al-Marzouqi, A.H.; Abu-Omar, M.M.; Khaleel, A.A. Klason Method: An Effective Method for Isolation of Lignin Fractions from Date Palm Biomass Waste. *Chem. Process Eng. Res.* **2018,** *57*, 46–58.
[59] Ihsan, B.R.; Shalas, A.F.; Elisabeth, Y.; Claudia, L.M.; Putri, A.R. Determination of Caffeine in Robusta Coffee Beans with Different Roasting Method Using UV-Vis Spectrophotometry. *Food. Res.* **2023,** *7* (6), 29–34. doi:10.26656/fr.2017.7(6).1006.
[60] Timell, T.E. Isolation of Galactoglucomannans from the Wood of Gymnosperms. *TAPPI* **1961,** *44* (2), 88–96.
[61] Nguyen, D.V.; Duong, C.T.T.; Vu, C.N.M.;, Nguyen, H.M.; Pham, T.T.; Tran-Thuy, T.M.; Nguyen, L.Q. Data on Chemical Composition of Coffee Husks and Lignin Microparticles as Their Extracted Product. *Data. Brief.* **2023,** *51*, 109781.
[62] Sayed, R.; Elmasri, M.; & Dhmees, M.; S, A. A Comparative Study of Particle Size Measurement of Silver,: Gold and Silica Sand Nanoparticles with Different Nanometrological Techniques. *Egypt. J. Chem.* **2023,** *66* (4), 385–393.
[63] Du, B.D.; Ngoc, D.T.B.; Thang, N.D.; Tuan, L.N.A.; Thach, B.D.; Hien, N.Q. Synthesis and in Vitro Antifungal Efficiency of Alginate-Stabilized Cu_2O-Cu Nanoparticles Against *Neoscytalidium dimidiatum* Causing Brown Spot Disease on Dragon Fruit Plants (*Hylocereus undatus*). *Vietnam Journal of Chemistry* **2019,** *57* (3), 318–323. doi:10.1002/vjch.201900022.
[64] Oktiawan, W.; & Zaman, B.. Use of a germination bioassay to test compost maturity in Tekelan Village, In E3S Web of Conferences, Semarang. 2018.
[65] Boadu, V.G.; Teye, E.; Amuah, C.L.; Lamptey, F.; Sam-Amoah, L.K. Portable NIR Spectroscopic Application for Coffee Integrity and Detection of Adulteration with Coffee Husk. *Processes* **1140,** *11* (4), 2023.
[66] Tello, J.; Viguera, M.; Calvo, L. Extraction of Caffeine from Robusta Coffee (*Coffea Canephora var. Robusta*) Husks Using Supercritical Carbon Dioxide. *J. Supercrit. Fluids.* **2011,** *59*, 53–60. doi:10.1016/j.supflu.2011.07.018.
[67] Gebresemati, M.; Gabbiye, N.; Sahu, O. Sorption of Cyanide from Aqueous Medium by Coffee Husk: Response Surface Methodology. *J. Appl. Res. Technol.* **2017,** *15* (1), 27–35. doi:10.1016/j.jart.2016.11.002.
[68] Collazo-Bigliardi, S.; Ortega-Toro, R.; Boix, A.C. Isolation and Characterisation of Microcrystalline Cellulose and Cellulose Nanocrystals from Coffee Husk and Comparative Study with Rice Husk. *Carbohydr. Polym.* **2018,** *191*, 205–215. doi:10.1016/j.carbpol.2018.03.022.
[69] Kabayo, S.M.; Kindala, J.T.; Nkanga, C.I.; Krause, R.W.; Taba, K.M. Preparation and Characterization of Solid Acid Catalysts Derived from Coffee Husks. *Int. J. Chem. Sci.* **2019,** *3* (6), 5–13.
[70] Gonçalves, B.M.M.; Camillo, M.D.O.; Oliveira, M.P.; Carreira, L.G.; Moulin, J.C.; Neto, H.F.; Oliveira, B.F.; Pereira, A.C.; Monteiro, S.N. Surface Treatments of Coffee Husk Fiber Waste for Effective Incorporation Into Polymer Biocomposites. *Polymers (Basel)* **2021**, *13* (19), 3428.
[71] Nallathambi, G.; Ramachandran, T.; Rajendran, V.; Palanivelu, R. Effect of Silica Nanoparticles and BTCA on Physical Properties of Cotton Fabrics. *Mater. Res.* **2011,** *14*, 552–559. doi:10.1590/S1516-14392011005000086.
[72] Ghani, N.N.A.; Saeed, M.A.; Hashim, I.H. Thermoluminescence (TL) Response of Silica Nanoparticles Subjected to 50 Gy Gamma Irradiation. *Malay. J. Fund. Appl. Sci.* **2017,** *13* (3), 178–180.
[73] Khalid, H.; Shamaila, S.; Zafar, N.; Shahzadi, S. Synthesis of Copper Nanoparticles by Chemical Reduction Method. *Sci. Int.* **2015,** *27* (4), 3085–3088.
[74] Phul, R.; Kaur, C.; Farooq, U.; Ahmad, T. Ascorbic Acid Assisted Synthesis, Characterization and Catalytic

Application of Copper Nanoparticles. *Int. J. Mater. Sci. Eng.* **2018,** *2* (4), 90–94.
[75] Kouti, M.; Matouri, L. Fabrication of Nanosized Cuprous Oxide Using Fehling's Solution. *Sci. Iran.* **2010,** *17* (1), 73–78.
[76] Yan, W.; Petkov, V.; Mahurin, S.M.; Overbury, S.H.; Dai, S. Powder XRD Analysis and Catalysis Characterization of Ultra-Small Gold Nanoparticles Deposited on Titania-Modified SBA-15. *Catal. Commun.* **2005,** *6* (6), 404–408. doi:10.1016/j.catcom.2005.04.004.
[77] Pabisch, S.; Feichtenschlager, B.; Kickelbick, G.; Peterlik, H. Effect of Interparticle Interactions on Size Determination of Zirconia and Silica Based Systems - A Comparison of SAXS, DLS, BET, XRD and TEM. *Chem. Phys. Lett.* **2012,** *521*, 91–97. doi:10.1016/j.cplett.2011.11.049.
[78] Jensen, H.; Pedersen, J.H.; J⊘rgensen, J.E.; Pedersen, J.S.; Joensen, K.D.; Iversen, S.B.; S⊘gaard, E.G. Determination of Size Distributions in Nanosized Powders by TEM, XRD, and SAXS. *J. Exp. Nanosci.* **2006,** *1* (3), 355–373. doi:10.1080/17458080600752482.
[79] Wang, Y.J.; Zhou, K.G. Effect of OH− on Morphology of Cu_2O Particles Prepared Through Reduction of Cu (II) by Glucose. *J. Central South Univ.* **2012,** *19* (8), 2125–2129. doi:10.1007/s11771-012-1254-4.
[80] Jolaei, M.M.; Montazer, M.; Rashidi, A.S.; Moghadam, M.B. Usage of Alkaline Glucose for Synthesis Copper Nano Particle on Polyester Fabric. *Ciênc. Nat.* **2015,** *37*, 63–70. doi:10.5902/2179460X20831.
[81] Tsao, R. Chemistry and Biochemistry of Dietary Polyphenols. *Nutrients* **2010,** *2* (12), 1231–1246. doi:10.3390/nu2121231.
[82] Cao, H.; Saroglu, O.; Karadag, A.; Diaconeasa, Z.; Zoccatelli, G.; Conte?Junior, C.A.; Gonzalez-Aguilar, G.A.; Ou, J.; Bai, W.; Zamarioli, C.M., et al. Available Technologies on Improving the Stability of Polyphenols in Food Processing. *Food Front.* **2021,** *2* (2), 109–139. doi:10.1002/fft2.65.
[83] Damaschin, R.; Popa, V.I.; Volf, I. A Suitable Method for Polyphenols Complexes with Copper. *Bul. Institt. Politehnic DIN IASI* **2018,** *64* (3), 19–29.
[84] Farhan, M.; Rizvi, A. Understanding the Prooxidant Action of Plant Polyphenols in the Cellular Microenvironment of Malignant Cells: Role of Copper and Therapeutic Implications. *Front. Pharmacol.* **2022,** *13* 929853.
[85] Ayalew, A.A.; Aragaw, T.A. Utilization of Treated Coffee Husk as low-Cost bio-Sorbent for Adsorption of Methylene Blue. *Adsorpt. Sci. Technol.* **2020,** *38* (5–6), 205–222. doi:10.1177/0263617420920516.
[86] Dufour, E. *Infrared Spectroscopy for Food Quality Analysis and Control*; 32. Academic Press: Cambridge, **2009**, 1–27.
[87] Veiga, T.R.L.A.; Lima, J.T.; Dessimoni, A.L.D.A.; Pego, M.F.F.; Soares, J.R.; Trugilho, P.F. Different Plant Biomass Characterizations for Biochar Production. *Cerne* **2017,** *23* (4), 529–536. doi:10.1590/01047760201723042373.
[88] Liu, Q.; Wang, S.; Zheng, Y.; Luo, Z.; Cen, K. Mechanism Study of Wood Lignin Pyrolysis by Using TG-FTIR Analysis. *J. Anal. Appl. Pyrolysis* **2008,** *82* (1), 170–177. doi:10.1016/j.jaap.2008.03.007.
[89] Kaur, K.; Kaur, K. Adsorptive Removal of Imazethapyr and Imazamox from Aqueous Solution Using Modified Rice Husk. *J. Cleaner Prod.* **2020**, *244*, 118699.
[90] Konneh, M.; Wandera, S.M.; Murunga, S.I.; Raude, J.M. Adsorption and Desorption of Nutrients from Abattoir Wastewater: Modelling and Comparison of Rice, Coconut and Coffee Husk Biochar. *Heliyon* **2021,** *7* (11), e08458.
[91] Zhang, Y.C.; Tang, J.Y.; Wang, G.L.; Zhang, M.; Hu, X.Y. Facile Synthesis of Submicron Cu_2O and CuO Crystallites from a Solid Metallorganic Molecular Precursor. *J. Cryst. Growth* **2006,** *294* (4), 278–282. doi:10.1016/j.jcrysgro.2006.06.038.
[92] Prakash, I.; Muralidharan, P.; Nallamuthu, N.; Venkateswarlu, M.; Satyanarayana, N. Preparation and Characterization of Nanocrystallite Size Cuprous Oxide. *Mater. Res. Bull.* **2007,** *42* (9), 1619–1624. doi:10.1016/j.materresbull.2006.11.038.
[93] Khan, M.A.; Ullah, M.; Iqbal, T.; Mahmood, H.; Khan, A.A.; Shafique, M.; Majid, A.; Ahmed, A.; Khan, N.A. Surfactant Assisted Synthesis of Cuprous Oxide (Cu_2O) Nanoparticles via Solvothermal Process. *Nanosci. Nanotechnol. Res.* **2015,** *3* (1), 16–22.
[94] Pham, T.H.; Viet, N.M.; Hoai, P.T.T.; Tung, N.H.; Tran, H.M.; Mapari, M.G.; Kim, T. Synthesis of Solar-Driven Cu-Doped Graphitic Carbon Nitride Photocatalyst for Enhanced Removal of Caffeine in Wastewater. *Environ. Res.* **2023,** *233*, 116483.
[95] León, G.R.; Aldás, M.B.; Guerrero, V.H.; Landázuri, A.C.; Almeida-Naranjo, C.E. Caffeine and Irgasan Removal from Water Using Bamboo, Laurel and Moringa Residues Impregnated with Commercial TiO_2 Nanoparticles. *MRS Adv.* **2019,** *4* (64), 3553–3567. doi:10.1557/adv.2020.33.
[96] Muthukumar, H.; Shanmugam, M.K.; Gummadi, S.N. Caffeine Degradation in Synthetic Coffee Wastewater Using Silverferrite Nanoparticles Fabricated via Green Route Using *Amaranthus Blitum* Leaf Aqueous Extract. *J. Water Process Eng.* **2020,** *36*, 101382.
[97] Shi, M.; Kwon, H.S.; Peng, Z.; Elder, A.; Yang, H. Effects of Surface Chemistry on the Generation of Reactive Oxygen Species by Copper Nanoparticles. *ACS Nano* **2012,** *6* (3), 2157–2164. doi:10.1021/nn300445d.
[98] He, W.; Zhou, Y.T.; Wamer, W.G.; Boudreau, M.D.; Yin, J.J. Mechanisms of the pH Dependent Generation of Hydroxyl Radicals and Oxygen Induced by Ag Nanoparticles. *Biomaterials* **2012,** *33* (30), 7547–7555. doi:10.1016/j.biomaterials.2012.06.076.
[99] Sawicka-Chudy, P., Sibiński, M., Wisz, G., Rybak-Wilusz, E., & Cholewa, M. Numerical Analysis and Optimization of Cu_2O/TiO_2, CuO/TiO_2, Heterojunction Solar Cells Using SCAPS. *J. Phys: Conf. Ser.* **2018**, 1033, 12002.
[100] Balık, M.; Bulut, V.; Erdogan, I.Y. Optical, Structural and Phase Transition Properties of Cu_2O, CuO and Cu_2O/CuO: Their Photoelectrochemical Sensor Applications. *Int. J. Hydrogen Energy* **2019,** *44* (34), 18744–18755.
[101] Miyasaki, Y.; Rabenstein, J.D.; Rhea, J.; Crouch, M.L.; Mocek, U.M.; Kittell, P.E.; Morgan, M.A.; Nichols, W.S.; Benschoten, M.M.V.; Hardy, W.D., et al. Isolation and Characterization of Antimicrobial Compounds in Plant

Extracts Against Multidrug-Resistant Acinetobacter Baumannii. *PLoS One* **2013,** *8* (4), e61594.

[102] Pagliarulo, C.; de Vito, V.; Picariello, G.; Colicchio, R.; Pastore, G.; Salvatore, P.; Volpe, M.G. Inhibitory Effect of Pomegranate (*Punica granatum* L.) Polyphenol Extracts on the Bacterial Growth and Survival of Clinical Isolates of Pathogenic *Staphylococcus Aureus* and *Escherichia coli*. *Food Chem.* **2016,** *190*, 824–831. doi:10.1016/j.foodchem.2015.06.028.

[103] Rangkadilok, N.; Tongchusak, S.; Boonhok, R.; Chaiyaroj, S.C.;, Junyaprasert, V.B.; Buajeeb, W.; Akanimanee, J.; Raksasuk, T.; Suddhasthira, T.; Satayavivad, J. *In Vitro* Antifungal Activities of Longan (*Dimocarpus longan* Lour.) Seed Extract. *Fitoterapia* **2012,** *83* (3), 545–553. doi:10.1016/j.fitote.2011.12.023.

[104] Marinaş, I.C.; Chifiriuc, C.; Oprea, E.; Lazăr, V. Antimicrobial and Antioxidant Activities of Alcoholic Extracts Obtained from Vegetative Organs of A. Retroflexus. *Roum. Arch. Microbiol. Immunol.* **2014,** *73* (1–2), 35–42.

[105] Pham, N.D.; Duong, M.M.; Le, M.V.; Hoang, H.A. Preparation and Characterization of Antifungal Colloidal Copper Nanoparticles and Their Antifungal Activity Against *Fusarium oxysporum* and *Phytophthora Capsici*. *C. R. Chim.* **2019,** *22* (11/12), 786–793. doi:10.1016/j.crci.2019.10.007.

[106] Chen, J.N.; Wu, L.T.; Kun, S.O.N.G.; Zhu, Y.S.; Wei, D.I.N.G. Nonphytotoxic Copper Oxide Nanoparticles are Powerful "Nanoweapons" That Trigger Resistance in Tobacco Against the Soil-Borne Fungal Pathogen *Phytophthora nicotianae*. *J. Integr. Agric.* **2022,** *21* (11), 3245–3262. doi:10.1016/j.jia.2022.08.086.

[107] Sawake, M.M., Moharil, M.P.; Ingle, Y.V.; Jadhav, P.V.; Ingle, A.P.; Khelurkar, V.C.; Paithankar, D.H.; Bathe, G.A.; Gade, A.K. Management of *Phytophthora Parasitica* Causing Gummosis in Citrus Using Biogenic Copper Oxide Nanoparticles. *J. Appl. Microbiol.* **2022,** *132* (4), 3142–3154. doi:10.1111/jam.15472.

[108] Guerrero, J.J.G.; Songkumarn, P.; Dalisay, T.U.; Pangga, I.B.; Organo, N.D. Toxicity of CuO and ZnO Nanoparticles and Their Bulk Counterparts on Selected Soil-Borne Fungi. *Agric. Nat. Resourc.* **2020,** *54*, 325–332.

[109] Shi, J.; Ye, J.; Fang, H.; Zhang, S.; Xu, C. Effects of Copper Oxide Nanoparticles on Paddy Soil Properties and Components. *Nanomaterials* **2018,** *8* (10), 839.

[110] Jośko, I.; Oleszczuk, P.; Dobrzyńska, J.; Futa, B.; Joniec, J.; Dobrowolski, R. Long-term Effect of ZnO and CuO Nanoparticles on Soil Microbial Community in Different Types of Soil. *Geoderma* **2019,** *352*, 204–212. doi:10.1016/j.geoderma.2019.06.010.

[111] Kumar, V.; Pandita, S.; Sidhu, G.P.S.; Sharma, A.; Khanna, K.; Kaur, P.; Bali, A.S.; Setia, R. Copper Bioavailability, Uptake, Toxicity and Tolerance in Plants: A Comprehensive Review. *Chemosphere* **2021,** *262*, 127810.

[112] Chen, G.; Li, J.; Han, H.; Du, R.; Wang, X. Physiological and Molecular Mechanisms of Plant Responses to Copper Stress. *Int. J. Mol. Sci.* **2022**, *23* (21), 12950.

[113] Zhao, X.; Chen, Y.; Li, H.; Lu, J. Influence of Seed Coating with Copper, Iron and Zinc Nanoparticles on Growth and Yield of Tomato. *IET Nanobiotechnol.* **2021,** *15*, 674–679. doi:10.1049/nbt2.12064.

[114] Hien, L.T.T.; Van, N.T. Effects of Nano Copper Used in Seed Treatment for Germination, Growth, and Productivity of Maize. *J. Biol.* **2018,** *4* (91), 40.

[115] Lee, W.M.; An, Y.J.; Yoon, H.; Kweon, H.S. Toxicity and Bioavailability of Copper Nanoparticles to the Terrestrial Plants Mung Bean (*Phaseolus radiatus*) and Wheat (*Triticum aestivum*): Plant Agar Test for Water-Insoluble Nanoparticles. *Environ. Toxicol. Chem: Int. J.* **2008,** *27* (9), 1915–1921.